



A mathematical model of a single seed oleosome

Luca Meacci^{a,*}, Vincenzo di Bari^b, Roberto Federico Ausas^a, Fernando Mut^c,
David Alistair Gray^b, Gustavo Carlos Buscaglia^a

^a Instituto de Ciências Matemáticas e de Computação, ICMC, Universidade de São Paulo, Avenida Trabalhador Sancarlene, 400, São Carlos (SP), CEP 13566-590, Brazil

^b Division of Food, Nutrition and Dietetics, School of Biosciences, University of Nottingham, Sutton Bonington Campus, LE12 5RD, UK

^c Bioengineering Department, George Mason University, 4400 University Drive, Fairfax, VA 22030, USA

ARTICLE INFO

Article history:

Received 19 June 2020

Received in revised form 24 September 2020

Accepted 25 September 2020

Available online 28 October 2020

MSC:

92C10

74L15

76Zxx

Keywords:

Mathematical modelling

Oleosome

Oil body

Lipid membrane

ABSTRACT

In this work we report for the first time a mathematical approach to model the behaviour of a single oleosome (oil body) within a seed cellular environment. To describe the behaviour of the oleosome membrane, we adopted a dynamical continuum model based on the principle of the virtual work where the intrinsic energy of the lipid membrane is assumed to obey the Canham–Helfrich model with the rheology of the viscous interface governed by the Boussinesq–Scriven law. To show the suitability of this approach to study the mechanical behaviour of oleosomes, we present some numerical simulations of a single oleosome deformation occurring under *in vivo* and *ex vivo* conditions. This work aims to show how the mathematical and computational modelling allows studying the impact of otherwise hard-to-measure physical quantities in this field of biological applications.

© 2020 The Authors. Published by Elsevier B.V. This is an open access article under the CC BY license (<http://creativecommons.org/licenses/by/4.0/>).

1. Introduction

In plant tissues energy is commonly stored in the form of carbohydrates and lipids. These energy resources support periods of active metabolism such seed germination and initial growth [1]. The most abundant lipid molecules in plants are triglycerides (or triacylglycerols), which are stored in specialised subcellular organelles called oleosomes, also referred to as “oil bodies”, “lipid bodies” or “spherosomes”. The size and composition of these organelles is affected by type of plant and of tissue (seeds, fruit mesocarps, leaves, microalgae), nutritional status and environmental factors [2]. In order to understand their biogenesis and functional role, oleosomes have been isolated from natural and genetically engineered plants and their structure and composition extensively investigated [2–9]. The oleosomes recovered from seeds are recognised to have a size mostly ranging between 0.2 to 2.5 μm [10]. Oleosome structure consists of a neutral lipid rich core stabilised by a monolayer membrane of phospholipids (PLs) and unique integral proteins [11]. The neutral lipid core includes the triacylglycerol molecules (TAG, molecules composed of three fatty acyl chains esterified to a glycerol backbone) and sterol esters. The PLs are oriented to expose the acyl moieties to the TAGs and the polar head group towards the external cytosol environment. Among the interfacial proteins, oleosin is the most abundant accounting for 75 – 90% of the total proteins, together with two minor proteins, caleosins and steroleosins [12]. In the accepted structural model of oleosomes found in angiosperm seeds, oleosin is believed to provide coverage to the PL head groups and to be exposed to the cytosol [13].

* Corresponding author.

E-mail address: luca.meacci@usp.br (L. Meacci).

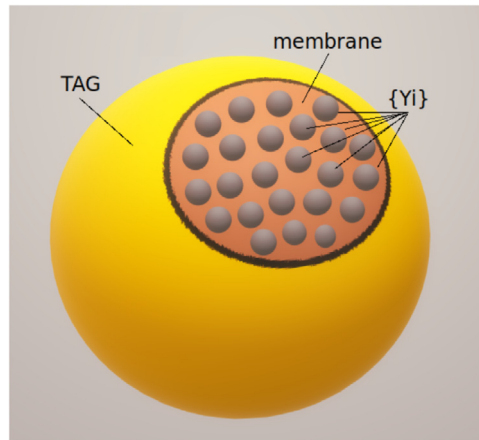


Fig. 1. Oleosome sketch with the triacylglycerol (TAG) matrix (in yellow) surrounded by a membrane (a portion of which in orange) of phospholipids and proteins. In the mathematical abstraction, the nodal points $\{Y^i\}$ (in grey) characterise the \mathcal{Y} membrane configuration.

In recent years oleosomes have attracted growing attention as sustainable natural ingredient for food and pharmaceutical applications. To fulfil this purpose, oleosomes are recovered using aqueous media from seeds (soybean, rapeseed, pumpkin, etc.) or nuts (pecan nut) and applied to manufacture dairy free alternatives to conventional milk and yogurts [14–17] as well as to produce natural cosmetics and pharmaceutical systems [18]. Despite its potential, molecular biology, food sciences, and chemistry have enabled much of the progress in this research area while mathematical studies are lacking. In recent years the mathematical and computational modelling of biological systems has significantly evolved proving to be a useful tool for the study of both biological membranes [19] and single cell phenomena [20]. In the case of living cells this kind of approach proved to be a suitable tool to understand and characterise the mechanical responses of cells subjected to both transient and dynamic loads [21] and continues to be a field of research for active and enthusiastic interest underpinning innovations of technologies of the future [22].

The goal of this paper is to address new interdisciplinary research questions: Can a mathematical modelling approach help to understand the physico-chemical and mechanical behaviour of oleosomes? And if so, can the tools of applied mathematics directly tackle some of the challenges associated with the study of oleosomes in applied bio-soft matter science? Therefore, the aim of this work was to test the suitability of a mathematical approach to model the behaviour of a single oleosome within a seed cellular environment. The long term objective of this work is to develop mathematical predictive tools to improve our knowledge of the mechanical and physico-chemical behaviour of oleosomes *in-vivo* (i.e., within seed environment) and *ex-vivo* (i.e., in technological applications).

2. Mathematical formulation

From a mathematical point of view, we can consider an oleosome as a mechanical system that has a configuration described by the state \mathcal{y} of the monolayer membrane of phospholipids and proteins. In Fig. 1 we show a scheme of our mathematical abstraction of an oleosome. The configuration \mathcal{y} is a configuration of the lipid membrane, which in the exact problem is an element of an infinite-dimensional manifold of possible membrane shapes. For numerical purposes, however, it is modelled as a finite-dimensional manifold spanned by generalised coordinates. In our case we adopt parameterisations that are defined by the positions of $N_{\mathcal{Y}}$ points, the *nodes* of the membrane model. The coordinates of any configuration \mathcal{y} are thus $\{Y^i\}_{i=1}^{N_{\mathcal{Y}}}$. We remark that the nodes do not correspond to any specific membrane constituent. From these coordinates the *geometrical position* of the membrane, $\Gamma(\mathcal{y}) = \{\mathbf{y} \in \mathbb{R}^3 \mid \mathbf{y} \text{ belongs to the membrane surface}\}$, can be reconstructed and, in the discrete case, being $\mathbf{F}^K(\boldsymbol{\xi}) = \sum_{j=1}^3 \mathbf{Y}^{C(K,j)} N^j(\boldsymbol{\xi})$, admits the explicit form

$$\Gamma(\mathcal{y}) = \{\mathbf{y} \in \mathbb{R}^3 : \mathbf{y} = \mathbf{F}^K(\boldsymbol{\xi}), \boldsymbol{\xi} \in \hat{K}, K = 1, \dots, M_{\mathcal{Y}}\} \tag{1}$$

where $C(\cdot, \cdot)$ is the connectivity matrix (that is, $C(K, j)$ is the index of the j th node of triangular element number K), $\hat{K} \in \mathbb{R}^2$ is the master element and $N^j : \hat{K} \rightarrow \mathbb{R}$ are the shape (or basis) functions (see also [23]). This discretisation of the surface leads to a faceted (triangulated) $\Gamma(\mathcal{y})$, over which a normal field \mathbf{n} (constant by element) is defined.

The instantaneous motion of the membrane particles is characterised by the rates of change of \mathcal{y} , as follows $\mathcal{W} = \frac{d\mathcal{y}}{dt}$. This means that the tracking of the surface is *Lagrangian* and that, in the discrete case, the velocity of the i th membrane node, $\mathbf{W}^i = \frac{dY^i}{dt}$, coincides with that of the lipid particle at $\mathbf{Y}^i(t)$. In this latter sentence “lipid particle” is to be understood not as a single molecule but as a small but macroscopic portion of membrane, in the spirit of Continuum Mechanics. Other

fields over $\Gamma(\mathcal{y})$ will be discretised in the same way as the geometry. More specifically, the vector field \mathbf{w} that represents the motion given the nodal velocities $\{\mathbf{W}^i\}$ is

$$\mathbf{w}(\mathbf{F}^K(\xi)) = \sum_{j=1}^3 \mathbf{W}^{C(K,j)} N^j(\xi). \tag{2}$$

Another important field over $\Gamma(\mathcal{y})$ is the mean curvature vector κ , equal to $H \mathbf{n}$, with H the mean curvature, with nodal values $\{\mathbf{K}^i\}_{i=1}^{N_Y}$ when discretised, so that

$$\kappa(\mathbf{y} \in \Gamma(\mathcal{y})) = \kappa(\mathbf{F}^K(\xi)) = \sum_{j=1}^3 \mathbf{K}^{C(K,j)} \mathcal{N}^j(\xi). \tag{3}$$

The geometrical equation for κ is the Laplace–Beltrami identity $-\Delta_\Gamma \mathbf{x} = \kappa$ that in weak form reads

$$\int_{\Gamma(\mathcal{y})} \nabla_\Gamma \mathbf{x} \cdot \nabla_\Gamma \zeta = \int_{\Gamma(\mathcal{y})} \kappa \cdot \zeta \tag{4}$$

where \mathbf{x} is the identity mapping,

$$\mathbf{x}(\mathbf{y}) = \mathbf{y}, \quad \mathbf{x}(\mathbf{F}^K(\xi)) = \sum_{j=1}^3 \mathbf{Y}^{C(K,j)} \mathcal{N}^j(\xi) \tag{5}$$

and $\nabla_\Gamma \mathbf{x}$ is the tangential projector \mathbb{P} ,

$$\mathbb{P} = \nabla_\Gamma \mathbf{x}(\mathbf{y}) = \mathbb{I} - \mathbf{n}(\mathbf{y}) \otimes \mathbf{n}(\mathbf{y}). \tag{6}$$

The energy of the proposed system is the intrinsic membrane energy ε_Y that clearly depends on \mathcal{y} . To study the evolution of the system, we will refer to the “principle of virtual work”, that, in our case, states that the work done by the energies yet defined for an admissible virtual variation of the configuration variables and the work done by the dissipative forces is equal to the work done by the external forces of the system [24]. The corresponding expression can therefore be formally written as

$$d_Y \varepsilon(\mathcal{y}) \bullet \delta \mathcal{y} + \mathcal{D}(\mathcal{y}, \mathcal{W}) \bullet \delta \mathcal{y} = \mathcal{F}_Y \bullet \delta \mathcal{y} \tag{7}$$

where

- $d_Y \varepsilon(\mathcal{y}) \bullet \delta \mathcal{y}$ is the infinitesimal change of energy $\delta \varepsilon$, when the state of the system is perturbed from \mathcal{y} to $\mathcal{y} + \delta \mathcal{y}$,
- the bullet \bullet is an appropriate duality product which will be detailed later (Section 2.1),
- $\mathcal{D}(\mathcal{y}, \mathcal{W}) \bullet (\delta \mathcal{y})$ is the dissipation of the system (i.e., the work of its internal dissipative forces), when the system is perturbed by $\delta \mathcal{y}$, and,
- $\mathcal{F}_Y \bullet \delta \mathcal{y}$ is the virtual work of external forces.

An explicit expression of the lipid layer model is presented below, describing in detail its mathematical formulation arising from Eq. (7).

2.1. Membrane energy and dissipation

Let us now consider the term $d_Y \varepsilon(\mathcal{y})$ of Eq. (7). The intrinsic energy ε_Y of the layer is given adopting the Canham–Helfrich model [25,26], i.e., considering the contribution of the curvature κ . The bending rigidity (or stiffness) is expressed by the parameter c_{CH} . Moreover, we introduce the addition due to the surface tension σ as follows

$$\varepsilon_Y(\mathcal{y}) = \int_{\Gamma(\mathcal{y})} \left(\frac{c_{CH}}{2} \|\kappa\|^2 + \sigma \right) d\Gamma. \tag{8}$$

Since the momentum equations are obtained from the virtual work principle, an expression for the variation of ε_Y is needed. This expression describes the consequence of a perturbation of the layer shape along a vector field \mathbf{z} defined on $\Gamma(\mathcal{y})$. The *shape derivative* of a functional \mathcal{J} in the direction of a virtual vector field \mathbf{z} is defined as

$$d\mathcal{J}(\mathcal{y}) \bullet \mathbf{z} = \lim_{\epsilon \rightarrow 0} \frac{\mathcal{J}(\mathcal{y} + \epsilon \mathbf{z}) - \mathcal{J}(\mathcal{y})}{\epsilon} \tag{9}$$

where in synthetic form $\mathcal{y} + \epsilon \mathbf{z} = \{\mathbf{Y} + \epsilon \mathbf{z}, \mathbf{Y} \in \mathcal{y}\}$. According to [27] for the Canham–Helfrich energy we obtain

$$d\varepsilon_Y(\mathcal{y}) \cdot \mathbf{z}_n = \int_{\Gamma(\mathcal{y})} \left[c_{CH} \left(-\Delta_\Gamma H - \frac{1}{2} H^3 + 2KH \right) + \sigma H \right] \mathbf{z}_n d\Gamma \tag{10}$$

with $\mathbf{z}_n = \mathbf{z} \cdot \mathbf{n}$ being the normal component of \mathbf{z} and \mathbf{n} the exterior normal to \mathcal{y} , Δ_Γ the Laplace–Beltrami operator, and H the mean curvature. Note that *tangential gradient* operator ∇_Γ is defined by $\nabla_\Gamma f = \mathbb{P} \nabla \mathbf{g}$, where $\mathbf{g} : \Gamma \rightarrow \mathbb{R}$

is any function and \widehat{g} an arbitrary extension of g to an open neighbourhood of $\Gamma \subset \mathbb{R}^3$. We remark that the curvature force occurs exclusively in the normal direction: tangential motions of \mathcal{Y} do not change its shape. With some calculations (see [27]) the (10) leads to

$$d\mathcal{E}_Y(\mathcal{Y}) \cdot \mathbf{z} = \int_{\Gamma(\mathcal{Y})} \left\{ c_{CH} \left[(\mathbb{I} - 2\mathbb{P})\nabla_\Gamma \boldsymbol{\kappa} : \nabla_\Gamma \mathbf{z} + \frac{1}{2}(\nabla_\Gamma \cdot \boldsymbol{\kappa})(\nabla_\Gamma \cdot \mathbf{z}) \right] + \sigma \nabla_\Gamma \right\} \cdot \mathbf{z} d\Gamma \tag{11}$$

where we remember \mathbf{x} is the identity mapping, $\boldsymbol{\kappa}$ obeys to the (4), and $\mathbb{P} = \mathbb{I} - \check{\mathbf{n}} \otimes \check{\mathbf{n}}$ is the tangential projector.

The dissipation function of the layer $\mathcal{D}(\mathcal{Y}, \mathbf{w}) \bullet \mathbf{z}$ is also needed. This is defined similarly to the viscous dissipation in volume fluids,

$$\mathcal{D}_Y(\mathcal{Y}, \mathbf{w}) \bullet \mathbf{z} = \int_{\Gamma(\mathcal{Y})} \boldsymbol{\Sigma} : D_\Gamma \mathbf{z} d\Gamma, \tag{12}$$

where $D_\Gamma \mathbf{z} = \frac{1}{2}\mathbb{P}(\nabla_\Gamma \mathbf{z} + \nabla_\Gamma \mathbf{z}^T)\mathbb{P}$ represents the virtual surface strain rate of field \mathbf{z} .

The rheology of a viscous interface Γ is governed by the Boussinesq–Scriven law [28–30], which is the tangential analogue to the Newtonian constitutive law, leading to the following viscous dissipative surface stress

$$\boldsymbol{\Sigma}_v = \lambda \nabla_\Gamma \cdot \mathbf{w} \mathbb{P} + 2 \mu D_\Gamma \mathbf{w}, \tag{13}$$

where λ and μ are surface viscosity coefficients. Consequently, we can write the dissipation term (12) as follows:

$$\mathcal{D}_Y(\mathcal{Y}, \mathbf{w}) \bullet \mathbf{z} = \int_{\Gamma(\mathcal{Y})} [\lambda \nabla_\Gamma \cdot \mathbf{w} \nabla_\Gamma \cdot \mathbf{z} + 2 \mu D_\Gamma \mathbf{w} : D_\Gamma \mathbf{z}] d\Gamma. \tag{14}$$

2.2. Lipid layer model

Over Γ we define the space of kinematically admissible motions, enforced with restrictions of local volume preservation, which is given by

$$\mathcal{V}(\Gamma(\mathcal{Y})) = \left\{ \mathbf{w} : \Gamma(\mathcal{Y}) \longrightarrow \mathbb{R}^3, \text{ s.e., } \int_{\Gamma(\mathcal{Y})} \mathbf{w} \cdot \mathbf{n} d\Gamma = 0 \right\}. \tag{15}$$

Specifically, the condition concerning the volume the osmotic equilibrium $\int_\Gamma \mathbf{w} \cdot \mathbf{n} d\Gamma = 0 \Rightarrow \frac{d\mathcal{V}}{dt} = \int_\Gamma \mathbf{w} \cdot \mathbf{n} d\Gamma = 0$. In discrete time, nevertheless, this condition is not satisfied exactly. This fact may lead to an accumulation of volume errors. The restriction can be therefore implemented as

$$\int_\Gamma \mathbf{w} \cdot \mathbf{n} d\Gamma - \frac{\mathcal{V}^* - \mathcal{V}(t)}{\tau_v \mathcal{V}(t)} = 0. \tag{16}$$

Such equation forces $\mathcal{V}(t)$ to the value \mathcal{V}^* with the characteristic time τ_v . The actual velocity field \mathbf{w} and any virtual ones \mathbf{v} must belong to $\mathcal{V}(\Gamma(\mathcal{Y}))$ for all configurations \mathcal{Y} of the surface.

In this context, the virtual work principle for the layer, with $\delta\mathcal{Y}$ represented by the vector field \mathbf{z} , reads

$$d\mathcal{E}_Y(\mathcal{Y}) \cdot \mathbf{z} + \mathcal{D}_Y(\mathcal{Y}, \mathbf{w}) \cdot \mathbf{z} = \int_{\Gamma(\mathcal{Y})} \mathbf{f} \cdot \mathbf{z} d\Gamma, \tag{17}$$

$\forall \mathbf{z} \in \mathcal{V}(\Gamma(\mathcal{Y}))$.

In the model adopted here we have greatly simplified the interaction with the surrounding fluid. In fact, the only force the surrounding fluid exerts on the layer comes from a uniform pressure difference, denoted by p , between the interior and exterior of Γ . We observe in fact that the (16) leads to an internal pressure p uniform which is expressed on the surface as a superficial force

$$\mathbf{f}_p = p\mathbf{n}. \tag{18}$$

With these deductions, we arrive at the following algebraic–differential problem: Solve

$$\frac{dY}{dt} = \mathbf{w}(Y, t), \tag{19}$$

where $(\mathbf{w}, \boldsymbol{\kappa}, p) \in \mathcal{W} \times \mathcal{Q} \times \mathcal{K} \times \mathbb{R}$ such that

$$\begin{aligned} & \int_\Gamma \lambda \nabla_\Gamma \cdot \mathbf{w} \nabla_\Gamma \cdot \mathbf{z} + 2 \mu D_\Gamma \mathbf{w} : D_\Gamma \mathbf{z} \\ & + c_{CH} \int_\Gamma \left[(\mathbb{I} - 2\mathbb{P})\nabla_\Gamma \boldsymbol{\kappa} : \nabla_\Gamma \mathbf{z} + \frac{1}{2}(\nabla_\Gamma \cdot \boldsymbol{\kappa})(\nabla_\Gamma \cdot \mathbf{z}) \right] \\ & = p \int_\Gamma \mathbf{z} \cdot \mathbf{n} + \int_\Gamma \mathbf{f}^{\text{ext}, \Gamma} \cdot \mathbf{z} - \int_\Gamma \sigma \nabla_\Gamma \cdot \mathbf{z} \end{aligned} \tag{20}$$

$$\int_{\Gamma} \boldsymbol{\kappa} \cdot \boldsymbol{\zeta} = \int_{\Gamma} \mathbb{P} : \nabla_{\Gamma} \boldsymbol{\zeta} \tag{21}$$

$$\int_{\Gamma} \boldsymbol{w} \cdot \boldsymbol{n} = \frac{\mathcal{V}^* - \mathcal{V}}{\tau_{\mathcal{V}}}, \tag{22}$$

$\forall (\mathbf{z}, \boldsymbol{\xi}, \boldsymbol{\zeta}) \in \mathcal{W} \times \mathcal{Q} \times \mathbf{K}$.

Above, \mathbf{K} is the mean-curvature-vector space, essentially equal to $(H^1(\Gamma))^3$. The space $\mathcal{Q} = L^2(\Gamma)$ corresponds to the surface tension field. The force field $\mathbf{f}^{\text{ext},\Gamma} : \Gamma \rightarrow \mathbb{R}^3$ encompasses all forces acting on the layer by external interventions.

3. Results and simulations

3.1. Numerical methods

For the layer continuum one we need to discretise it. We consider triangulation surfaces in 3D space, which for a fixed mesh connectivity are uniquely described by the vector \mathbf{Y} of vertex positions. Time is discretised so that a sequence of triangulation surfaces $\Gamma^0, \Gamma^1, \dots, \Gamma^n, \dots$ are computed, corresponding to vertex positions $\mathbf{Y}^0, \mathbf{Y}^1, \dots, \mathbf{Y}^n, \dots$. Following the approach proposed by Rodrigues et al. [31], on each Γ^n we define the piecewise-affine finite element space $P_1^n = \{\mathbf{f} \in C^0(\Gamma^n) : \mathbf{f}|_K \text{ is affine}, \forall K \text{ triangle in } \Gamma^n\}$ and the approximation spaces for velocity, surface and curvature $\mathbf{W}_h^n = (P_1^n)^3 / \mathbb{R}$, $\mathcal{Q}_h^n = P_1^n$, $\mathbf{K}_h^n = (P_1^n)^3$. We define $\Delta t = t_{n+1} - t_n$ and we update the nodal positions in a Lagrangian way, specifically, $\mathbf{Y}^{j,n+1} = \mathbf{Y}^{j,n} + \mathbf{W}^{j,n+1} \delta t$. With these definitions we can arrive at a fully discrete *non-linear* problem corresponding to the weak formulation of the system (20)–(22) only introducing one temporal stabilisation term $-\int_{\Gamma^n} \tau_k \nabla_{\Gamma} \mathbf{w}_h^{n+1} : \nabla_{\Gamma} \boldsymbol{\zeta}_h$, suggested by Bänsch [32] and described also in [31], for which the usual choice is $\tau_k = \delta t$. In Sections 3.2 and 3.3 we present some preliminary results of some numerical resolution with finite elements method (FEM) of this fully-discrete numerical model. We avoid a detailed description of the parameters setup to focus on the qualitative observation of the results. Evidences show the uncertainty of evaluating dynamical parameters as well material quantities such as the surface tension [33]. The simulations presented in the following sections aim at illustrating the possibilities and the potentiality of the model to shed light over the role and measuring of the physical quantities. This model can be used in combination with laboratory work.

3.2. Hypothesis, equilibrium, and lipid layer stress

We discretise the surface of the oleosome in a surface of triangles, i.e., in a mesh with 642 nodes 1280 edges. For the time discretisation we adopted a time step Δt of the magnitude order of 10^{-3} time unit. We refer to an ellipsoidal initial form of the oleosome with an average radius of the order of 1, corresponding to and initial volume and initial surface area of $V_0 = 4.15$ and $A_0 = 13.24$, respectively. Also we put an arbitrary Canham–Helfrich constant $c_{\text{CH}} = 1$ that corresponds to establish the energy unit to 1 kT. We recall that according our model we assume condition (a) of constant volume, due to the fact that we consider the oil fluid inside the membrane incompressible, and the hypothesis (b) of variable surface area that guarantees the deformability of the lipid layer.

With respect to the set-up of dynamical parameters, we take $\mu = 1$ since any other value would only change the time scale but not the equilibrium configuration. Since it has not been experimentally proven otherwise, the ratio μ/λ is set to 1, which gives similar significance to shear and dilatational dissipation actions. It should be kept in mind that here we are focusing on natural and/or laboratory studies (as hydration or drying out) which are slow processes. A reasonable choice of surface tension σ corresponds to that such that the characteristic length L (which is R) of the system is of the order of $\sqrt{\frac{c_{\text{CH}}}{\sigma}}$. The value of σ affects the internal pressure value at equilibrium, for instance in the case of a sphere of $p = \frac{2\sigma}{R}$. We will focus on the possibility of evaluating the internal pressure value because in the laboratory process of oleosomes extraction, the pressure influences the probability of breaking them and therefore the quality of the final extract. Extracting intact oleosomes is of paramount importance to formulate stable natural oil-in-water emulsions for food and pharma applications. Another factor possibly responsible for the fragmentation of the lipid membranes during the extraction process is the development of regions with very large *bending moment*, defined as $M = -2 c_{\text{CH}} H$ [34].

Let us first introduce the simulation with our model of a relaxation process, i.e., starting from a initial configuration and in absence of external forces, we allow the system to evolve towards the equilibrium state. In Fig. 2 we display the time evolution of the interfacial layer and the magnitude of the mean curvature vector $\boldsymbol{\kappa}$ in the case with $\sigma = 1$. The top-left panel corresponds to the initial configuration. It appears clear that, although the oleosome starts from a stressed condition (assuming it has deformed by external forces as shown in the top left panel), it converges with time to its equilibrium condition which is spherical and therefore with constant average curvature (bottom right panel). From a physical and mathematical point of view this behaviour is due to the tendency of the system to go to a condition of minimal energy. In Fig. 3 we can see as the energy decreases over time achieving a “plateau” level modelled using different values of σ . This configuration corresponds also to a minimum value of the pressure that the core liquid oil exerts from inside towards the membrane (pressure data shown in the centre-panel of Fig. 3). We note that these results are consistent with the previous discussion over the internal pressure.

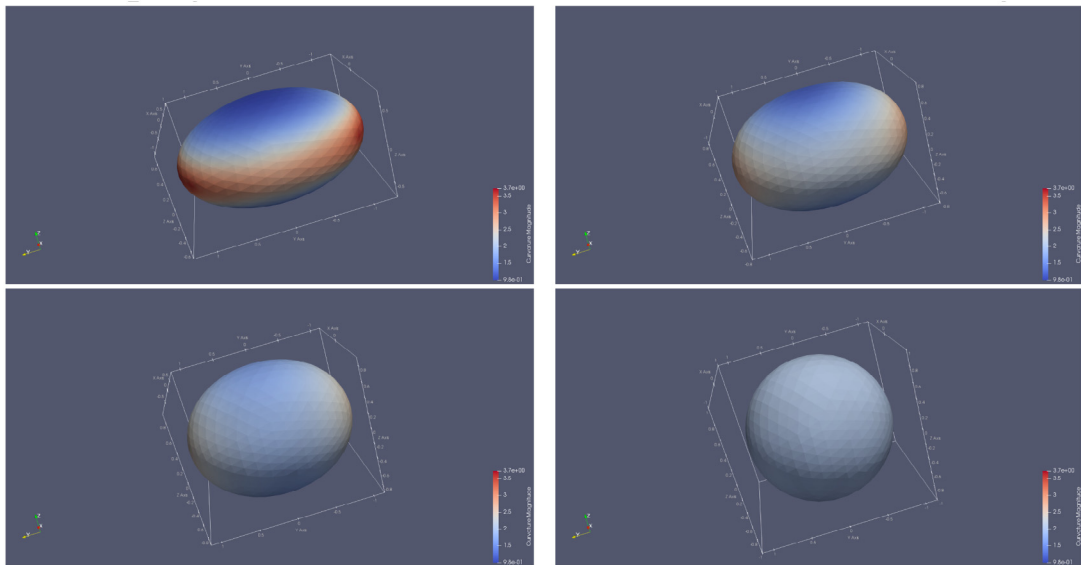


Fig. 2. Panels of the evolution of the lipid layer during the relaxation process: at initial condition ($t = 0$, top left panel) and at time $t = 0.26$ (top right), $t = 0.73$ (bottom left) and $t = 3.85$ (bottom right).

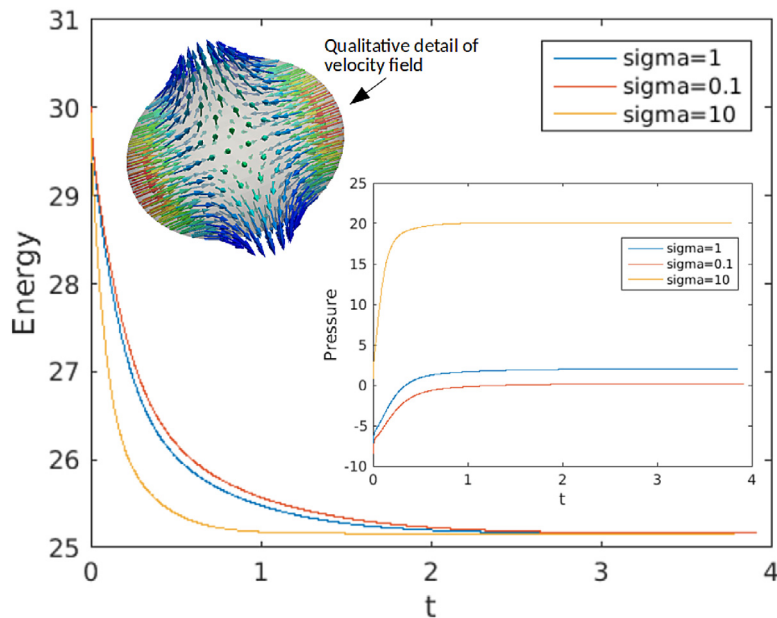


Fig. 3. Lipid layer energy and internal olesome pressure (insert) over time. A qualitative detail about the velocity field is shown.

As we can see from the previous results (Fig. 3), the surface tension influences the velocity of degrowth of energy but not its equilibrium value, a fact which is coherent because the organelle (without external perturbations) tends to a sphere. Let us now suppose to subject the lipid membrane to a compression stress between two rigid planes. In this case the evolution of the internal pressure is not of trivial calculation. In Fig. 4 we report some snapshots of the evolution of the membrane shape and the corresponding solution for the internal pressure over time and for different values of the interfacial tensions. We are also interested in evaluating the bending moment during the process. In Fig. 4 on the bottom panel we show the evolution of the maximum magnitude of the bending moment evaluated by the model (with $\sigma = 1$, because with the other values of σ the graph is analogous). These simulations results allow to study the impact of otherwise hard-to-measure physical quantities as well as gaining information over the possible breaking limit of the interfacial layer under stress.

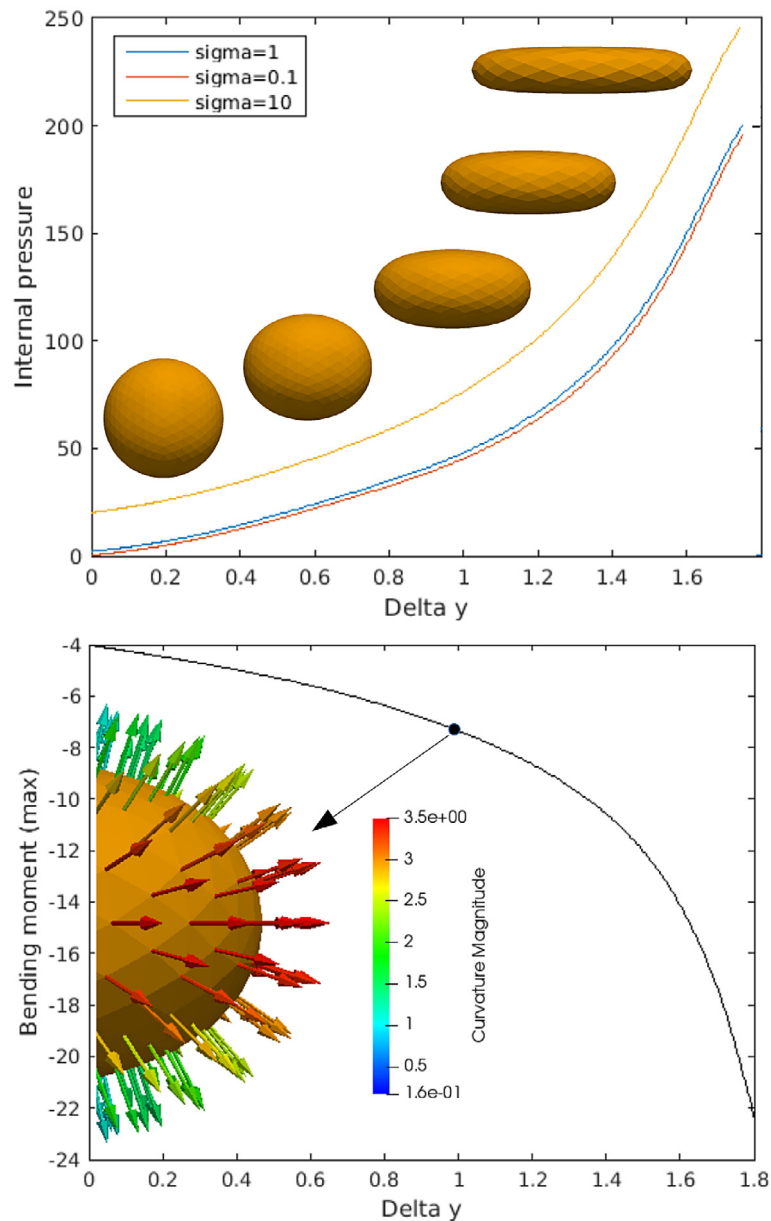


Fig. 4. Time evolution of the internal pressure (top) and the bending moment (below) exercising compression stress.

3.3. Senescence: a virtual experiment

Compression stress is not only a key element of laboratory (or industrial) processes but also of natural phenomena. In order to show the potentiality of this new approach we present here a virtual experiment of seeds senescence. As it can be seen from the microscopy picture of Peng and Tzen [35] of a sesame seed (Fig. 5), it is observed experimentally that inside the seed evolving towards its the senescence phase (when water is lost) the oleosomes come into contact with each other and take polygonal shapes to allow a better packing within the available space.

We simulated the natural phenomenon while applying our model to a virtual senescence experiment to reproduce the events occurring *in vivo*. For sake of example, one oleosome is hypothesised to be surrounded by four other rigid organelles, increasingly approaching towards the centre and exerting a contact interaction. The inset plotted in Fig. 5 shows as (from an initial spherical shape) the oleosome, due to influence of the interaction with the approaching organelles, assumes the peculiar shape in agreement with what is observed experimentally in seed tissues. The apparently polygonal shape reveals (as shown in a blue-scale line around the layer) a complex curvature distribution, with flat parts

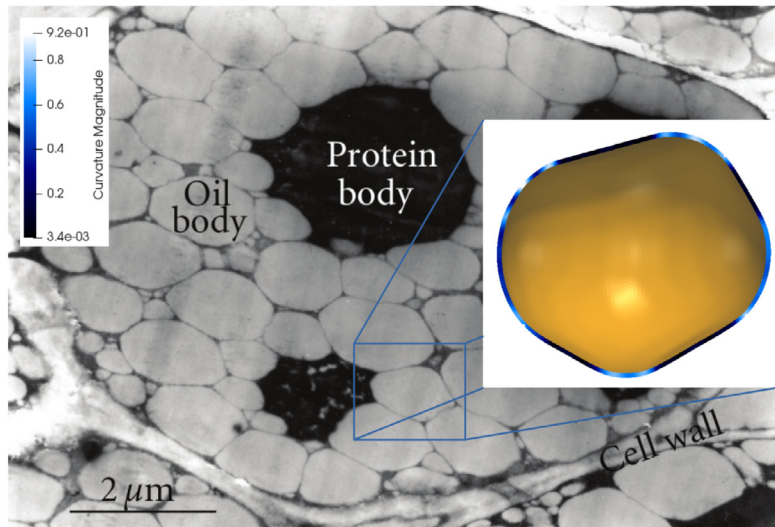


Fig. 5. Electron microscopy of a cell in a mature sesame seed (adopted and modified from [35]). The typical polygonal shape assumed by oleosomes due to the interaction/contact with other organelles can be observed. The inset contains a digital reproduction of an oleosome displaying its polygonal shape.

of the membrane, others with an almost circular curvature (where interaction with external organelles is negligible) and areas with maximum curvatures (and consequently, as we have seen, maximum bending moments).

4. Conclusions and opportunities for future developments

In this work we presented for the first time a model of a single oleosome, providing a detailed mathematical formulation. Although only qualitative, these results show the potential of such approach. Therefore, the main outcome of this interdisciplinary concept study is to offer a starting point for a new research line combining a mathematical modelling approach with laboratory experimental results for oleosome research.

Understanding and modelling the behaviour of oleosomes is relevant from both a fundamental and applied science point of view. These organelles display *in-vivo* the remarkable ability to preserve their structural integrity over a wide temperature and hydration range [12,36,37], which triggers fundamental questions referring to the membrane fluid behaviour and mechanical properties under those environmental conditions. We believe mathematical modelling could provide new insights to understand oleosomes behaviour during seed maturation, storage and energy mobilisation. Understanding their *ex-vivo* (i.e., following extraction from plant seed tissues) functionalities is also pivotal for food and pharmaceutical applications; oleosomes could be used as natural alternative for emulsion formulations (i.e., ice cream, mayonnaise, and salad dressings). This approach would allow reducing synthetic emulsifiers usage, processing costs and environmental impacts providing support to tackle global sustainability challenges.

Declaration of competing interest

The authors declare that they have no known competing financial interests or personal relationships that could have appeared to influence the work reported in this paper.

Acknowledgements

The work was supported by grants from the School of Biosciences (Sutton Bonington Campus) of the University of Nottingham (UK), and from the Instituto Nacional de Ciência e Tecnologia - Medicina Assistida por Computação Científica (Brazil) financed by FAPESP (Brazil) (Grant 2014/50889-7). This research was developed making use of the computational resources (Euler cluster) of the Center for Mathematical Sciences Applied to Industry (CeMEAI). L. M. acknowledges CAPES (Brazil) for receiving economic support (PROEX-9740044/D).

References

- [1] Murphy DJ, Vance J. Mechanisms of lipid-body formation. *Trends Biochem Sci* 1999;24(3):109–15.
- [2] Huang AH. Oil bodies and oleosins in seeds. *Annu Rev Plant Biol* 1992;43(1):177–200.
- [3] Brasaemle DL, Wolins NE. Packaging of fat: an evolving model of lipid droplet assembly and expansion. *J Biol Chem* 2012;287(4):2273–9.

- [4] Zweytick D, Athenstaedt K, Daum G. Intracellular lipid particles of eukaryotic cells. *Biochim Biophys Acta (BBA)-Rev Biomembr* 2000;1469(2):101–20.
- [5] Napier JA, Stobart AK, Shewry PR. The structure and biogenesis of plant oil bodies: the role of the er membrane and the oleosin class of proteins. *Plant Mol Biol* 1996;31(5):945–56.
- [6] Bourgeois C, Gomaai A, Lefèvre T, Cansell M, Subirade M. Interaction of oil bodies proteins with phospholipid bilayers: A molecular level elucidation as revealed by infrared spectroscopy. *Int J Biol Macromol* 2018.
- [7] Wanner G, Formanek H, Theimer R. The ontogeny of lipid bodies (sphaerosomes) in plant cells. *Planta* 1981;151(2):109–23.
- [8] Huang A. Oleosins and oil bodies in seeds and other organs. *Plant Physiol* 1996;110(4):1055.
- [9] Nikiforidis CV. Structure and functions of oleosomes (oil bodies). *Adv Colloid Interface Sci* 2019;102039.
- [10] Chapman KD, Dyer JM, Mullen RT. Biogenesis and functions of lipid droplets in plants thematic review series: lipid droplet synthesis and metabolism: from yeast to man. *J Lipid Res* 2012;53(2):215–26.
- [11] Tzen J. Seed oil bodies of sesame and their surface proteins, oleosin, caleosin, and steroleosin. *Sesame, Genus Sesamum* 2011;48:187–200.
- [12] Tzen JT. Integral proteins in plant oil bodies. *ISRN Bot* 2012;2012.
- [13] Tzen J, Huang A. Surface structure and properties of plant seed oil bodies. *J Cell Biol* 1992;117(2):327–35.
- [14] De Chirico S, di Bari V, Foster T, Gray D. Enhancing the recovery of oilseed rape seed oil bodies (oleosomes) using bicarbonate-based soaking and grinding media. *Food Chem* 2018;241:419–26.
- [15] Adams GG, Imran S, Wang S, Mohammad A, Kok MS, Gray DA, Channell GA, Harding SE. Extraction, isolation and characterisation of oil bodies from pumpkin seeds for therapeutic use. *Food Chem* 2012;134(4):1919–25.
- [16] Zhang P, Bari VD, Briars R, Taher ZM, Yuan J, Liu G, Gray D. Influence of pecan nut pretreatment on the physical quality of oil bodies. *J Food Qual* 2017;2017.
- [17] Nikiforidis CV, Matsakidou A, Kiosseoglou V. Composition, properties and potential food applications of natural emulsions and cream materials based on oil bodies. *RSC Adv* 2014;4(48):25067–78.
- [18] Bettini S, Vergara D, Bonsegna S, Giotta L, Toto C, Chieppa M, Maffia M, Giovinazzo G, Valli L, Santino A. Efficient stabilization of natural curcuminoids mediated by oil body encapsulation. *RSC Adv* 2013;3(16):5422–9.
- [19] Steigmann DJ. The role of mechanics in the study of lipid bilayers, Vol. 577. Springer; 2017.
- [20] Bao G, Suresh S. Cell and molecular mechanics of biological materials. *Nat Mater* 2003;2(11):715.
- [21] Lim C, Zhou E, Quek S. Mechanical models for living cells—a review. *J Biomech* 2006;39(2):195–216.
- [22] Rajagopal V, Holmes WR, Lee PVS. Computational modeling of single-cell mechanics and cytoskeletal mechanobiology. *Wiley Interdiscip Rev: Syst Biol Med* 2018;10(2):e1407.
- [23] Tasso IV, Buscaglia GC. A finite element method for viscous membranes. *Comput Methods Appl Mech Engrg* 2013;255:226–37.
- [24] Lanczos C. The variational principles of mechanics. 4th edn. Toronto: Toronto University Press; 1970.
- [25] Canham PB. The minimum energy of bending as a possible explanation of the biconcave shape of the human red blood cell. *J Theoret Biol* 1970;26(1):611N777–761N881.
- [26] Helfrich W. Elastic properties of lipid bilayers: theory and possible experiments. *Z Naturforsch C* 1973;28(11–12):693–703.
- [27] Bonito A, Nochetto RH, Pauletti MS. Parametric FEM for geometric biomembranes. *J Comput Phys* 2010;229(9):3171–88.
- [28] Boussinesq M. Sur l'existence d'une viscosité superficielle, dans la mince couche de transition séparant un liquide d'une autre fluide contigue. *Ann Chim Phys* 1913;29:349–57.
- [29] Scriven L. Dynamics of a fluid interface equation of motion for Newtonian surface fluids. *Chem Eng Sci* 1960;12(2):98–108.
- [30] Gross S, Reusken A. Numerical methods for two-phase incompressible flows, Vol. 40. Springer Science & Business Media; 2011.
- [31] Rodrigues DS, Ausas RF, Mut F, Buscaglia GC. A semi-implicit finite element method for viscous lipid membranes. *J Comput Phys* 2015;298:565–84.
- [32] Bänsch E. Finite element discretization of the Navier–Stokes equations with a free capillary surface. *Numer Math* 2001;88(2):203–35.
- [33] White SH. Small phospholipid vesicles: internal pressure, surface tension, and surface free energy. *Proc Natl Acad Sci* 1980;77(7):4048–50.
- [34] Guckenberger A, Gekle S. Theory and algorithms to compute helfrich bending forces: A review. *J Phys: Condens Matter* 2017;29(20):203001.
- [35] Peng C-C, Tzen JT. Analysis of the three essential constituents of oil bodies in developing sesame seeds. *Plant Cell Physiol* 1998;39(1):35–42.
- [36] Frandsen GI, Mundy J, Tzen JT. Oil bodies and their associated proteins, oleosin and caleosin. *Physiol Plant* 2001;112(3):301–7.
- [37] Barre A, Simplicien M, Cassan G, Benoist H, Rougé P. Oil bodies (oleosomes): Occurrence, structure, allergenicity. *Rev Fr Allergol* 2018.